Journal of Molecular Catalysis A: Chemical 321 (2010) 92–100

Contents lists available at ScienceDirect

Journal of Molecular Catalysis A: Chemical

journal homepage: www.elsevier.com/locate/molcata

The effect of immobilization on the catalytic activity of molybdenum η^3-allyldicarbonyl complexes with nitrogen donor ligands bearing N–H groups

Marta S. Saraiva[a], Carla D. Nunes[a], Teresa G. Nunes[b], Maria José Calhorda[a,*]

[a] Departamento de Química e Bioquímica, CQB, Faculdade de Ciências da Universidade de Lisboa, Campo Grande, 1749-016 Lisboa, Portugal
[b] Centro de Química Estrutural, Instituto Superior Técnico, Av. Rovisco Pais, 1049-001 Lisboa, Portugal

ARTICLE INFO

Article history:
Received 13 October 2009
Received in revised form
21 December 2009
Accepted 4 February 2010
Available online 11 February 2010

Keywords:
Molybdenum
Mesoporous materials
Catalysis
Epoxidation
Dinitrogen ligands
Allyl complexes

ABSTRACT

The two complexes $[Mo(\eta^3\text{-}C_3H_5)Br(CO)_2(L)]$ (L = **L1**, **C1**, and **L2**, **C2**), where **L1** and **L2** are the ligands 2-(2′-pyridyl)imidazole (**L1**, pym) and 2-(2′-pyridyl)benzimidazole (**L2**, pyb) were immobilized in mesoporous MCM-41 and in Mg/Al hydrotalcite (HTC), in order to obtain new heterogeneous catalysts. Both the ligands and the complexes reacted with MCM-41 functionalized with a chloropropyl pendant arm; in the first approach, the immobilized ligands were then allowed to react with $[Mo(\eta^3\text{-}C_3H_5)Br(CO)_2(NCMe)_2]$ to afford supported **C1** and **C2**. While spectroscopic data, DRX, and nitrogen isotherm adsorptions revealed the similarity of the two kinds of materials, and the preservation of the MCM characteristic structure, elemental analysis showed that the stepwise approach (ligand + complex precursor) allowed the introduction of a much larger amount of molybdenum. The attempts at immobilization of the complexes in HTC were less successful. Neither the deprotonated ligands or complexes were able to intercalate between the material layers, the experimental evidence suggesting the intercalation of OH^- anions and the adsorption of the deprotonated ligands or complexes on the outside of the clay. Both materials exhibited higher activities in the epoxidation of cyclooctene and styrene, in the presence of TBHP, than the free complexes in homogeneous conditions, with conversions close to 100% for both substrates, in the MCM based materials prepared through a stepwise route.

1. Introduction

The development of new and efficient heterogeneous catalysts, combining the selectivity of homogeneous catalysts with the advantages of heterogeneous processes, namely easy recovery of products and recycling of the promoter, continues to be a priority in chemistry [1,2].

Active centers may be immobilized in several ways, depending on the binding between active center and support. The family of the silicon based porous MCM materials, developed by Mobil in 1992 [3,4], led to new paths for the reaction between suitable precursors with the SiOH groups in the internal walls of the large surface of the hexagonally ordered parallel channels. The applications of the resulting materials containing inorganic active centers in several fields, from catalysis to optoelectronics, followed [1,5–7]. Typical approaches for such reactions include direct grafting, where a functionalized complex reacts with the OH groups, or tethering where a step by step route is followed, starting by reaction between the walls and a functionalized organic molecule (ligand) which then binds the metal center [8,9]. When no suitable function is available, a spacer can be used [6,10].

Other kinds of porous materials may be more suitable, depending on the nature of the metal complex and the reactions to perform. Some layered materials can be used with success to immobilize ionic species by means of electrostatic interactions. In particular, layered double hydroxides are clays with a structure based on hydroxides, such as $Mg(OH)_2$. Some Mg^{2+} cations in the edge-sharing $Mg(OH)_6$ octahedra layer may be replaced by M^{3+} cations, yielding a charge unbalance that requires anions. These and water molecules occupy the interlayer space. In hydrotalcite (HTC), the cationic layer contains Mg^{2+} and Al^{3+}, with compositions $[M_{1-x}{}^{2+}M_x{}^{3+}(OH)_2](A^{m-})_{x/m} \cdot nH_2O$ (M^{2+} = Mg^{2+}, Zn^{2+}, Ni^{2+}, etc., M^{3+} = Al^{3+}, Cr^{3+}, Ga^{3+}, etc.) [11,12], and the ratio between cations (x) is associated with the interlayer distance in the structure. Anion exchange provides the easiest route for functionalization of the clay, and may also change this distance, depending on the size of the anion. A common procedure, more efficient than direct anion exchange, consists of calcination of the precursor clay, usually containing carbonate, followed by rehydration in the presence of another anion, leading to swelling of the structure [11a,12,13]. The intercalated anion may then react with inorganic species [14]. Substitution of the cations is another possibility for modifying and functionalizing clays. Some authors have prepared double hydrox-

* Corresponding author. Tel.: +351 217500196; fax: +351 217500088.
E-mail addresses: mssaraiva@fc.ul.pt (M.S. Saraiva), cmnunes@fc.ul.pt (C.D. Nunes), pcteresa@popsrv.ist.utl.pt (T.G. Nunes), mjc@fc.ul.pt (M.J. Calhorda).

1381-1169/$ – see front matter © 2010 Elsevier B.V. All rights reserved.
doi:10.1016/j.molcata.2010.02.008

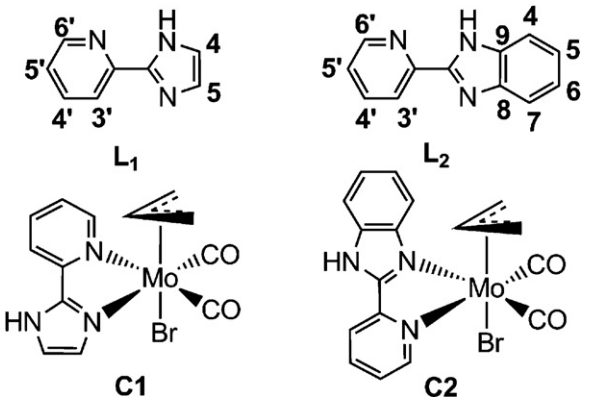

Scheme 1. Schematic representation of ligands $\mathbf{L_1}$ and $\mathbf{L_2}$, and complexes **C1** and **C2**.

ides directly in presence of the anions designed to belong to the final structure [15]. Both the HTC material by itself and functionalized with metal active centers have shown catalytic activity in several reactions, namely aziridination of oxiranes [16] and olefin polymerization [14].

In this work, the two molecules 2-(2′-pyridyl)imidazole ($\mathbf{L_1}$, pym) and 2-(2′-pyridyl)benzimidazole ($\mathbf{L_2}$, pyb) were chosen as ligands (see Scheme 1) to functionalize MCM-41 and a Mg/Al HTC and to react with the Mo(II) complex $[Mo(\eta^3\text{-}C_3H_5)X(CO)_2(NCMe)_2]$ [17]. Organometallic complexes in general are very versatile as homogeneous catalysts in a wide variety of reactions, as well as in many other applications [18]. The Mo(II)$(\eta^3\text{-}C_3H_5)(CO)_2$ derivatives and their W(II) analogues have displayed activity in catalysis [19], namely imine aziridation [20], phosphine oxidation [21], allylic alkylations [22], and, more recently as precursors in olefin oxidation. $[Mo(\eta^3\text{-}C_3H_5)X(CO)_2(NCMe)_2]$ (X = Cl, Br) and some of their derivatives containing 1,4-diaza-1,3-butadienes or other bidentate nitrogen donor ligands promoted the selective olefin epoxidation in the presence of *t*-butyl hydroperoxide (TBHP) [23]. Active species usually contain Mo(VI), as in the industrial ARCO-Halcon process for homogeneous olefin epoxidation with TBHP as source of oxygen [24]. These catalysts have been shown to be as active as other well described Mo(II) precursors [25], with high conversions and turnover frequencies, and maintaining a high activity in the second run.

Since the two complexes $[Mo(\eta^3\text{-}C_3H_5)Br(CO)_2(L)]$ (L = $\mathbf{L_1}$, **C1**, and $\mathbf{L_2}$, **C2**, Scheme 1) have been previously described and their activity as precursors in the epoxidation of cyclooctene and styrene determined [26], we studied their immobilization in MCM-41 and a Mg/Al HTC and their catalytic activity in the same reaction, in order to evaluate the effect of the support on the catalytic activity and to compare it with related systems.

2. Experimental

2.1. General

All reagents and ligand 2-(2′-pyridyl)benzimidazole $\mathbf{L_2}$ were obtained from Aldrich and used as received. Commercial grade solvents were dried and deoxygenated by standard procedures (Et_2O, THF, and toluene over Na/benzophenone ketyl; CH_2Cl_2 over CaH_2), distilled under nitrogen, and kept over 4 Å molecular sieves. The ligand 2-(2′-pyridyl)imidazole ($\mathbf{L_1}$) [27] and the complexes $[Mo(\eta^3\text{-}C_3H_5)Br(CO)_2(NCCH_3)_2]$ [17b] and $[Mo(\eta^3\text{-}C_3H_5)Br(CO)_2(L)]$ (L = $\mathbf{L_1}$, **C1**, and $\mathbf{L_2}$, **C2**) [26] were prepared according to literature methods. MCM-41 and derivatized materials were synthesized by adopting a methodology previously described, using $[(C_{14}H_{33})N(CH_3)_3]Br$ as templating agent [10]. Prior to the grafting experiment, physisorbed water was removed from calcined (540 °C for 6 h under air) **MCM** (**1**) by heating at 180 °C in vacuum (10^{-2} Pa) for 2 h.

FTIR spectra were obtained as KBr pellets (complexes) and Diffuse Reflectance (DRIFT) measurements (materials) on a Nicolet 6700 in the 400–4000 cm^{-1} range using 1 cm^{-1} resolution. Powder XRD measurements were taken on a Philips PW1710 using Cu Kα radiation filtered by graphite. ^1H and ^{13}C solution NMR spectra were obtained with a Bruker Avance 400 spectrometer.

Solid state NMR measurements were performed at room temperature on a Bruker MSL 300P spectrometer operating at 59.60 and 75.47 MHz for the observation of ^{29}Si and ^{13}C resonances, respectively. The standard magic angle spinning (MAS) cross-polarization–dipolar decoupling RF pulse sequence (CP-DD) was used under about 4 kHz spinning rate. For the acquisition of ^{29}Si spectra, 5 ms contact time, 6 s recycling delay, and a number of scans always higher than 3000 were selected; the Hartmann–Hahn condition was optimized using tetrakis-trimethylsilylsilane and tetramethylsilane (TMS) was the external reference to set the chemical shift scale ($\delta = 0$). ^{13}C spectra were recorded with 2 ms contact time, 4 s recycling delay and a number of scans higher than 900. The Hartmann–Hahn condition was optimized using glycine, also the external reference to set the chemical shift scale (^{13}CO at 176.1 ppm).

The N_2 adsorption/desorption measurements were obtained in an automatic apparatus (ASAP 2010; Micromeritics). BET specific surface areas (S_{BET}, p/p^0 from 0.03 to 0.13) and specific total pore volume, V_p were estimated from N_2 adsorption isotherms measured at 77 K. The pore size distributions (PSD) were calculated by the BJH method using the modified Kelvin equation with correction for the statistical film thickness on the pore walls [28,29]. The statistical film thickness was calculated using Harkins–Jura equation in the p/p^0 range from 0.1 to 0.95. Microanalyses (C, N, H, and Mo) were performed at the University of Vigo, Spain.

2.2. Catalytic studies

The complexes and materials were tested in the epoxidation of *cis*-cyclooctene (cy8) and styrene (sty), using *t*-butylhydroperoxide (TBHP) as oxidant. The catalytic oxidation tests were carried out at 328 K under normal atmosphere in a reaction vessel equipped with a magnetic stirrer and a condenser. In a typical experiment the vessel was loaded with olefin (100%), internal standard (DBE), catalyst (1%), oxidant (200%), and 3 mL of solvent. Addition of the oxidant determines the initial time of the reaction. The course of the reactions was monitored by quantitative GC-analysis by collecting samples at 10, 30 min, 1 h and 1 h 30 min, then at 2, 4, 6, 8, and 24 h of reaction. These samples were treated as described previously prior to injection in the GC column [26].

2.2.1. Epoxidation of cis-cyclooctene

Cis-cyclooctene (800 mg, 7.3 mmol), 800 mg dibutyl ether (internal standard), 1 mol% of catalyst, 2.65 mL of TBHP (5.5 M in *n*-decane) and 3 mL of CH_2Cl_2.

2.2.2. Epoxidation of styrene

Styrene (800 mg, 7.7 mmol), 800 mg dibutyl ether (internal standard), 1 mol% of catalyst, 2.65 mL of TBHP (5.5 M in *n*-decane) and 3 mL of CH_2Cl_2.

MCM-Pr-Cl

2.0 mL of 3-(chloropropyl)-trimethoxysilane was added to a suspension of 1 g of MCM-41 (**1**) in 30 mL of toluene, and allowed to reflux for 24 h. The yellow suspension was filtered, washed with 4× 20 mL dichloromethane, and dried under vacuum. Different samples are indicated by *.

MCM-Pr-Cl (**2**)

Anal. Found: C 7.40, H 1.89%.

IR (KBr, ν/cm^{-1}): 3445 (bd, s), 2959 (m), 1638 (w), 1084 (vs), 813 (s).

^{13}C CP/MAS (DD) NMR (δ ppm): 9.0 (Si–CH_2), 26.1 (–CH_2–), 46.1 (Cl–CH_2).

^{29}Si CP/MAS (DD) NMR (δ ppm): −46.3 (T^1), −56.9 (T^2), −67.5 (T^3), −101.6 (Q^3), −109.0 (Q^4).

MCM-Pr-Cl* (**2***)

Anal. Found: C 8.36, H 1.97%.

IR (KBr, ν/cm^{-1}): 3417 (bd, s), 2954 (m), 2849 (m), 1627 (w), 1243 (vs), 1059 (vs), 817 (s).

^{13}C CP/MAS (DD) NMR (δ ppm): 9.2 (Si–CH_2), 26.1 (–CH_2–), 45.9 and less intense signal at 49.1 (Cl–CH_2).

^{29}Si CP/MAS (DD) NMR (δ ppm): −48.3 (T^1), −57.7 (T^2), −67.5 (T^3), −101.6 (Q^3), −109.4 (Q^4).

MCM-Pr-Cl** (**2****)

Anal. Found: C 8.36, H 1.87%.

IR (KBr, ν/cm^{-1}): 3424 (bd, s), 2955 (m), 2850 (m), 1622 (w), 1244 (vs), 1070 (vs), 813 (s).

MCM-Pr-L$_n$ (**L$_n$ = L$_1$** (**3**), **L$_2$** (**4**))

The ligand (4 mmol) was dissolved in dichloromethane, and then triethylamine (4.8 mmol) was added. 1 g of **MCM-Pr-Cl** (**2**) was added to this solution, at 0 °C, and then left at room temperature for 12 h. The suspension was filtered, washed with 2× 20 mL dichloromethane, and dried under vacuum.

MCM-Pr-L$_1$ (**3**) (from **MCM-Pr-Cl** (**2**))

Anal. Found: C 2.27, H 10.51, N 1.33%.

IR (KBr, ν/cm^{-1}): 3418 (bd, s), 3006 (vw), 2959 (w), 1671 (w), 1597 (w), 1461 (vw), 1080 (vs), 803 (s).

^{13}C CP/MAS (DD) NMR (δ ppm): 7.8, 9.9 (Si–CH_2), 26.3 (–CH_2–), 45.7 (N–CH_2).

^{29}Si CP/MAS (DD) NMR (δ ppm): −58.5 (T^2), −66.7 (T^3), −101.2 (Q^3), −109.4 (Q^4).

MCM-Pr-L$_2$ (**4**) (from **MCM-Pr-Cl** (**2***))

Anal. Found: C 10.60, H 2.30, N 0.89%.

IR (KBr, ν/cm^{-1}): 3418 (bd, s), 3010 (vw), 2960 (w), 1628 (w), 1446 (vw), 1242 (vs), 1077 (vs), 808 (s).

^{13}C CP/MAS (DD) NMR (δ ppm): 7.4, 9.7 (Si–CH_2), 26.1 (–CH_2–), 45.2 (N–CH_2).

^{29}Si CP/MAS (DD) NMR (δ ppm): −58.5 (T^2), −67.5 (T^3), −101.2 (Q^3), −109.0 (Q^4).

MCM-Pr-L$_n$-Mo (**L$_n$ = L$_1$** (**5a**), **L$_2$** (**5b**)

0.750 g of **MCM-Pr-L$_n$** were added to a solution of [Mo(η^3-C_3H_5)Br(CO)$_2$(NCMe)$_2$] (**A**) (1 mmol) in dichloromethane. The mixture was stirred for one day in inert atmosphere, filtered, washed with dichloromethane, and dried under vacuum.

MCM-Pr-L$_1$-Mo (**5a**)

Anal. Found: C 9.15, H 2.10, N 0.88, Mo 6.21%.

IR (KBr, ν/cm^{-1}): 3422 (bd, s), 3011 (vw), 2949 (w), 1939 (s), 1847 (s), 1651 (vs), 1440 (w), 1242 (s), 1078 (vs), 804 (s).

^{13}C CP/MAS (DD) NMR (δ ppm): 8.0, 9.5 (Si–CH_1), 26.3 (–CH_2–), 46.7 (N–CH_2).

^{29}Si CP/MAS (DD) NMR (δ ppm): −48.3 (less intense, T^1), −57.7 (T^2), −66.7 (T^3), −101.6 (Q^3), −108.6 (Q^4).

MCM-Pr-L$_2$-Mo (**5b**)

Anal. Found: C 8.76, H 2.02, N 0.34, Mo 3.07%.

IR (KBr, ν/cm^{-1}): 3419 (bd, s), 3015 (vw), 2942 (w), 1941 (s), 1859 (s), 1623 (vs), 1442 (w), 1242 (s), 1077 (vs), 803 (s).

^{13}C CP/MAS (DD) NMR (δ ppm): 8.0, 9.5 (Si–CH_2), 26.3 (–CH_2–), 46.9 (N–CH_2).

^{29}Si CP/MAS (DD) NMR (δ ppm): −56.9 (T^2), −66.3 (T^3), −101.2 (Q^3), −109.4 (Q^4).

MCM-Pr-MoL$_n$ (**L$_n$ = L$_1$ (6a), L$_2$ (6b)**)

The complex (4 mmol) was dissolved in DMF, and then triethylamine (4.8 mmol) was added. 1 g of **MCM-Pr-Cl**** (**2****) was added to this solution, at 0 °C, and left at room temperature for 12 h. The suspension was filtered, washed with 2× 20 mL DMF and dried under vacuum.

MCM-Pr-MoL$_1$ (from **MCM-Pr-Cl**** (**2****)) (**6a**)

Anal. Found: C 11.65, H 2.20, N 2.54, Mo 0.44%.

IR (KBr, ν/cm^{-1}): 3406 (bd, s), 3010 (vw), 2938 (w), 1941 (s), 1853 (s), 1663 (vs), 1390 (m), 1242 (s), 1067 (vs), 802 (s).

MCM-Pr-MoL$_2$ (from **MCM-Pr-Cl**** (**2****2**)) (**6b**)

Anal. Found: C 10.10, H 1.85, N 1.57, Mo 0.52%.

IR (KBr, ν/cm^{-1}): 3336 (bd, s), 2939 (w), 1941 (w), 1870 (s), 1662 (vs), 1496 (s), 1439 (s), 1418 (s), 1390 (m), 1314 (w), 1240 (s), 1063 (vs), 800 (s).

HTC-MoL$_n$ (**L$_n$ = L$_1$** (**7**), **L$_2$** (**8**))

A solution of NaOH (2 mmol) in 20 mL of desionized water (type II) was added to a solution of the complex (2.8 mmol) in 15 mL of DMF. A suspension of 1 g of clay HTC in 25 mL of DMF was then added to this solution, and heated at 70 °C for 48 h. The clay was filtered, washed with 3× 20 mL deionized water and dried under vacuum.

HTC-Mo L$_1$ (**7**)

Anal. Found: C 2.83,H 2.56, N 0.53, Mo 3.32%.

IR (KBr, ν/cm^{-1}): 3464 (bd, s), 1935 (m), 1839 (m), 1584 (s), 1368 (vs), 942 (vs), 682 (s).

^{13}C CP/MAS (DD) NMR (δ ppm): 38.6, 170.3 (CO) (major signals).

HTC-Mo L$_2$ (**8**)

Anal. Found: C 13.13,H 2.57, N 2.61, Mo 7.08%.

IR (KBr, ν/cm^{-1}): 3455 (bd, s), 1932 (m), 1837 (m), 1608 (s), 1462 (w), 1428 (w), 1367 (vs), 951 (vs), 749 (s).

^{13}C CP/MAS (DD) NMR (δ ppm): 59.9 and 73.7 (allylic carbons), 118.5 (4), 123.3 (6), 127.8 (5′), 144.5 (9), 146.6 (10), 148.9 (6′), 156.6, 170.5 (CO) (major signals).

3. Results and discussion

3.1. MCM-41 materials

The ligands 2-(2′-pyridyl)imidazole (**L$_1$**, pym) and 2-(2′-pyridyl)benzimidazole (**L$_2$**, pyb) and the complexes [Mo(η^3-C_3H_5)Br(CO)$_2$(L)] (L = **L$_1$**, **C1**, and **L$_2$**, **C2**, Scheme 1) were used for the preparation of two families of composite materials, one based on mesoporous MCM-41 and the second on Mg/Al hydrotalcite (HTC). In both hosts, two synthetic strategies were tested, namely the introduction of the whole complexes, or the loading of the ligands followed by the reaction with [Mo(η^3-C_3H_5)Br(CO)$_2$(NCMe)$_2$]. Both procedures have been used before [8].

The pure siliceous MCM-41 (**MCM**) parent material was obtained by a template approach [30], and was afterwards derivatized by following two strategies as depicted in Scheme 2, both synthetic pathways starting with the same first step. This consisted of the grafting of a spacer, chloropropyltrimethoxysilane, on the walls of the **MCM** material, affording the material **MCM-Pr-Cl** (**2**).

In the first route, the stepwise preparation of the final material was achieved by introducing the ligand **L$_1$** or **L$_2$** in the presence of triethylamine, so that the resulting anion would react with the pendant chloropropyl chains inside the pores of MCM, as shown in the right side of Scheme 2. The two new materials **MCM-Pr-L$_n$** (L$_n$ = **L$_1$**, **3**, or **L$_2$**, **4**) were obtained. Subsequent reaction with [Mo(η^3-C_3H_5)Br(CO)$_2$(CH_3CN)$_2$] afforded the materials **MCM-Pr-L$_n$-Mo** by substitution of the nitrile ligands by the immobilized ligands of **MCM-Pr-L$_n$**. The prepared materials **MCM-Pr-L$_1$-Mo** (**5a**) and **MCM-Pr-L$_2$-Mo** (**5b**) contained approximately 6.21 wt% Mo (0.65 mmol g^{-1}) and 3.07 wt% Mo (0.32 mmol g^{-1}), respectively.

The second route, depicted on the left side of Scheme 2, was carried out by deprotonating the whole complexes [Mo(η^3-C_3H_5)Br(CO)$_2$L] (L = **L$_1$** or **L$_2$**) with triethylamine in DMF. The deprotonated complexes **C1** and **C2** reacted with the pendant

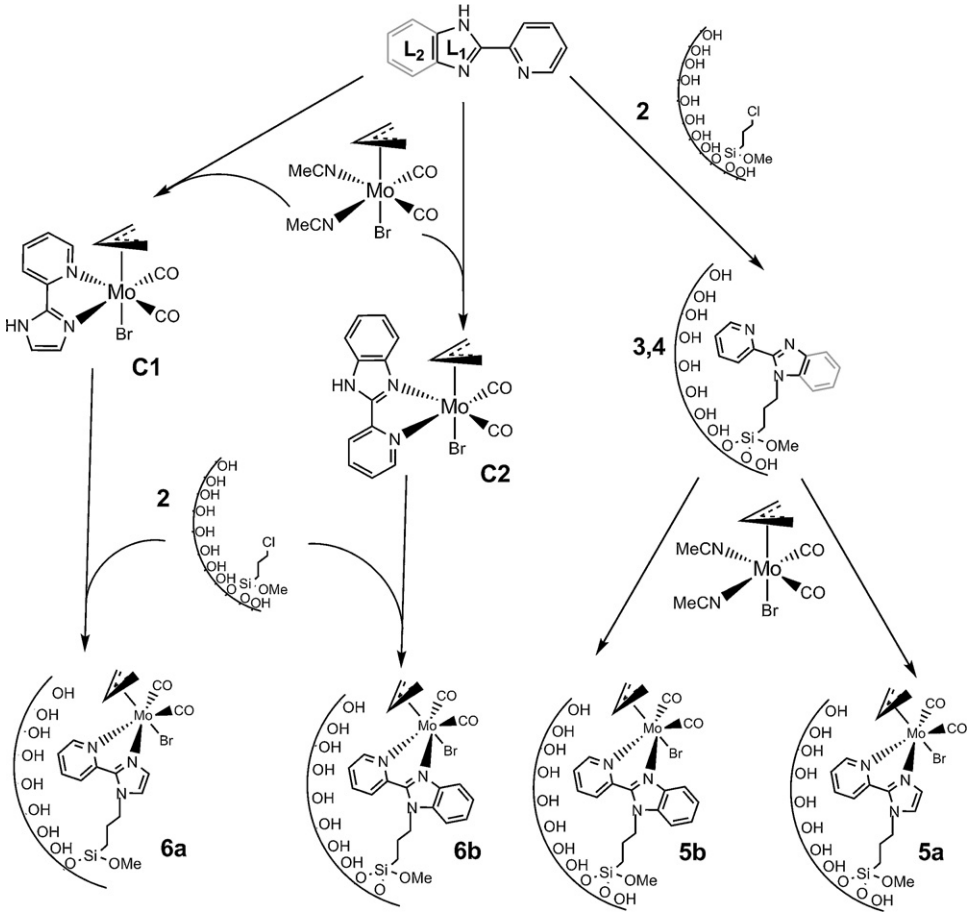

Scheme 2. Schematic procedure for the synthesis of **MCM** materials.

chloropropyl chains of **MCM-Pr-Cl** affording the materials **MCM-Pr-Mo L_1** (**6a**) and **MCM-Pr-MoL_2** (**6b**), with metal loadings of approximately 0.44 and 0.52 wt% Mo, corresponding to 0.045 and 0.054 $mmol_{Mo}\,g^{-1}$, respectively.

These results indicate that the stepwise introduction of the complex is more efficient, leading to a much higher amount of molybdenum in the new materials. This effect has been described before, and the difference is more striking when the complexes are larger [8].

The powder XRD patterns of **MCM-Pr-L_2-Mo** (**5b**) and **MCM-Pr-MoL_2** (**6b**) are given in Fig. 1. The pattern of the parent, calcined material **MCM** (**1**), shows four reflections in the 2θ range 2–10°, indexed to a hexagonal cell as (1 0 0), (1 1 0), (2 0 0), and (2 1 0). The d value of the (1 0 0) reflection is 35.2 Å, corresponding to a lattice constant of $a = 40.6$ Å ($=2d_{100}/\sqrt{3}$). The positions of the peaks of **MCM-Pr-Cl** (**2**), after functionalizing the walls of the parent host material **MCM** with chloropropyltrimethoxysilane, remain almost unchanged, suggesting the retention of the long range hexagonal symmetry of the host material. The powder patterns also remain unchanged for material **MCM-Pr-L_2-Mo** (**5b**). A reduction of the peaks intensities is observed in the case of **MCM-Pr-L_2** (**4**), and becomes more relevant in the molybdenum rich **MCM-Pr-L_2-Mo** (**5b**). This is not interpreted as a loss of crystallinity, but rather to a reduction in the X-ray scattering contrast between the silica walls and pore-filling material, a situation well described in the literature [31,32], and also observed for other types of materials [14].

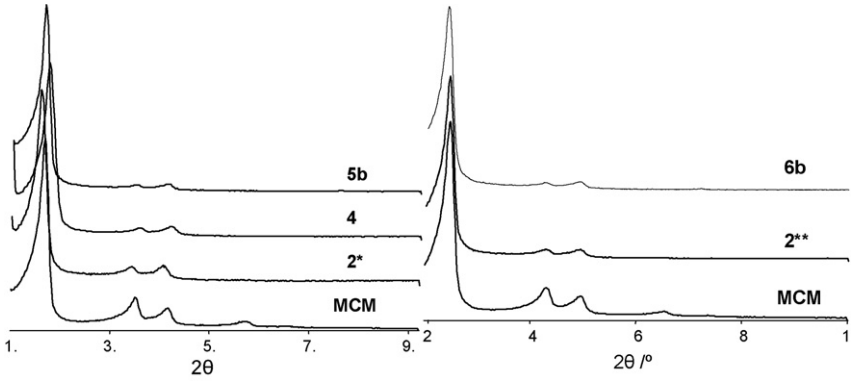

Fig. 1. Powder XRD of materials **MCM**, **MCM-Pr-Cl** (**2**), **MCM-Pr-L_2** (**4**), **MCM-Pr-L_2-Mo** (**5b**), and **MCM-Pr-MoL_2** (**6b**), prepared by both pathways, using ligand **L_2**.

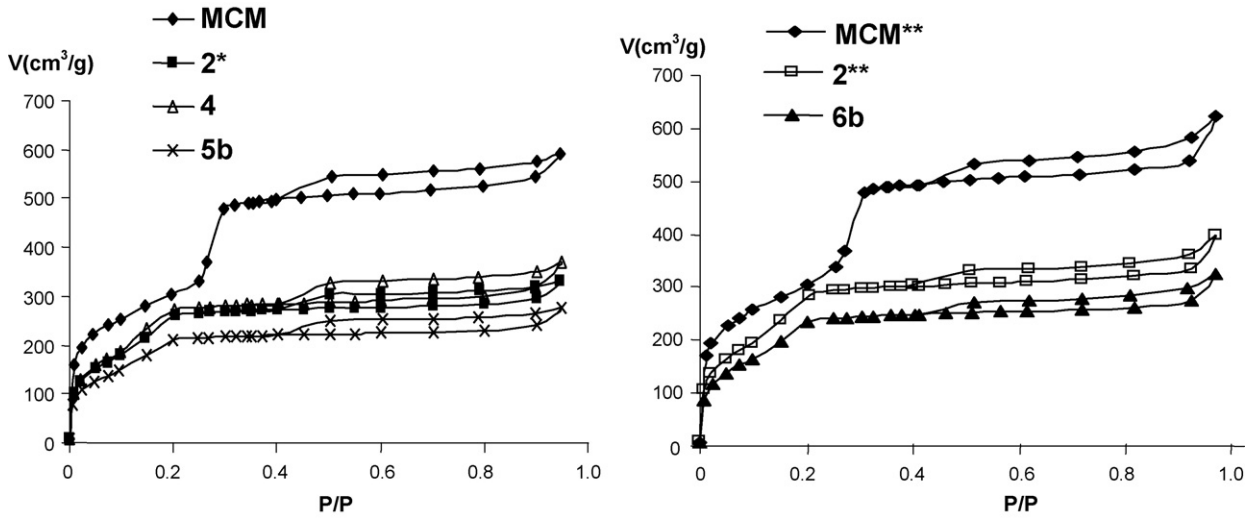

Fig. 2. Nitrogen adsorption studies of materials **MCM**, **MCM-Pr-Cl** (**2**), **MCM-Pr-L$_2$** (**4**), **MCM-Pr-L$_2$-Mo** (**5b**), and **MCM-Pr-MoL$_2$** (**6b**), at 77 K.

When the complexes **C1** and **C2** were directly introduced in the parent **MCM** material to form **MCM-Pr-MoL$_2$** (**6b**), a reduction in the peaks intensities was also observed, though not as drastic (Fig. 1, right) as the reduction observed in the stepwise pathway (Fig. 1, left). Indeed, in this way, smaller molecules (the ligands **L$_1$** and **L$_2$**) are introduced allowing a better coverage of the surface, and reacting then with a Mo source. The introduction of the bulkier complexes **C1** and **C2** will be less effective, owing to their larger size.

Nitrogen adsorption studies at 77 K revealed that the pristine **MCM** (**1**) sample exhibits a reversible type IV isotherm (Fig. 2), characteristic of mesoporous solids (pore width between 2 and 50 nm, according to the IUPAC) [33]. The calculated textural parameters (S_{BET} and V_p) of this material agree with literature data (Table 1) [34,35]. The capillary condensation/evaporation steps appear in the 0.20–0.40 relative pressures range, and the sharpness of this step reflects the uniform pore size.

The isotherm of the functionalized material **MCM-Pr-Cl*** (**2***) reveals much lower N_2 uptake, accounting for decrease in ΔV_p (29–45%) and a concomitant variation in S_{BET}. These results indicate that immobilization of the ligand on the internal silica surface was accomplished (Fig. 2, Table 1). Introduction of the ligands **L$_1$** and **L$_2$** inside the pores induces only a very slight variation, whereas the introduction of the metal moieties provokes a further decrease. The same observations are true for the parallel synthetic pathway where the Mo complexes **C1** and **C2** were introduced as a whole (Fig. 2, right). The relative decrease in S_{BET} and V_p relative to **MCM** is in agreement with the decrease of the p/p^0 coordinates of the inflection points of the isotherms after post-synthesis treatments [36]. The height of the capillary condensation steps, which is related to the volume of pore space confined by absorbate film on the pore walls, is smaller in the case of the modified materials. Furthermore, the maxima of the PSD curves determined by the BJH method, d_{BJH}, decrease concomitantly (Table 1).

The presence of functional groups characteristic of [Mo(η^3-C_3H_5)Br(CO)$_2$(L)] in the materials was checked by FTIR spectroscopy. The stretching vibrations modes of the mesoporous framework (Si–O–Si) of the grafted material **MCM-Pr-Cl*** (**2***) are observed at around 1240, 1070, and 810 cm^{-1}, as in the parent **MCM**, while new bands appear at ca. 2950 and 2850 cm^{-1}, assigned to the ν(C–H) stretching of the aliphatic linear chain in **MCM-Pr-Cl**. The introduction of the ligands **L$_1$** and **L$_2$** in the stepwise pathway leads to the appearance of the ν(C=N) stretching modes at 1671 and 1597 cm^{-1} (in **MCM-Pr-L$_1$**) and 1628 cm^{-1} (in **MCM-Pr-L$_2$**). After binding the complexes, the bands assigned to the asymmetric vibration mode of Si–O–Si are still observed at 1241, 1066, and 806 cm^{-1} in **MCM-Pr-L$_1$-Mo** (**5a**), while the ν(C=N) stretching modes of the ligands are shifted to 1651 cm^{-1} in **MCM-Pr-L$_1$-Mo** (**5a**) and to 1623 cm^{-1}in **MCM-Pr-L$_2$** (**4**). The ν(C≡O) stretching modes of the *cis*-C≡O groups are observed at around 1939 and 1847 cm^{-1} for **MCM-Pr-L$_1$-Mo** (**5a**) and 1941 and 1859 cm^{-1} for **MCM-Pr-L$_2$-Mo** (**5b**), slightly shifted from the values in the free

Table 1
Textural parameters for host and composite materials from N_2 isotherms at 77 K.

Sample	d_{100} (Å)	S_{BET} (m^2 g^{-1})	ΔS_{BET}[a] (%)	V_p (cm^3 g^{-1})	ΔV_p[b] (%)	d_{BJH}[c] (nm)
MCM (**1**)	36.5	1122	–	0.98	–	3.20
MCM-Pr-Cl (**2**)	35.7	1148	2	0.70	−29	2.66
MCM-Pr-L$_1$ (**3**)	36.4	841	−25	0.51	−48	2.66
MCM-Pr-L$_1$-Mo (**5a**)	34.4	673	−40	0.39	−60	2.65
MCM* (**1***)	35.2	1091	–	0.92	–	3.26
MCM–Pr-Cl* (**2***)	36.7	906	−17	0.51	−45	2.85
MCM-Pr-L$_2$ (**4**)	34.6	1004	−8	0.57	−38	2.66
MCM-Pr-L$_2$-Mo (**5b**)	35.7	753	−31	0.42	−54	2.65
MCM** (**1****)	35.0	1096	–	0.96	–	3.26
MCM-Pr-Cl** (**2****)	35.5	1011	−8	0.62	−35	2.65
MCM-Pr-MoL$_1$ (**6a**)	35.8	867	−21	0.49	−49	2.65
MCM-Pr-MoL$_2$ (**6b**)	36.6	829	−24	0.50	−48	2.86

[a] Variation of surface area in relation to parent **MCM**.
[b] Variation of total pore volume in relation to parent **MCM**.
[c] Median pore width determined by the BJH method.

complexes (1933 and 1839 cm^{-1} in **C1**; 1934 and 1853 cm^{-1} in **C2**). The same frequencies are observed for the materials **MCM-Pr-MoL$_1$** (**6a**) and **MCM-Pr-MoL$_2$** (**6b**) obtained by the second route and containing the same immobilized species.

The materials were also characterized by ^{13}C CP MAS-DD and ^{29}Si CP MAS-DD solid state NMR. The solid state ^{13}C CP MAS-DD NMR spectra (Fig. S1, Supporting Information) of **MCM-Pr-Cl*** (**2***), **MCM-Pr-L$_2$** (**4**) and **MCM-Pr-L$_2$-Mo** (**5b**) materials are quite similar, since the spectra are dominated by the resonances of the propyl chain. These signals appear at ca. 9.2 ($Si–CH_2$), 26.1 ($CH_2–CH_2–CH_2$), and 45.9 ($Cl–CH_2$) ppm in **2***, and the last one shifts to ca. 45.2 ppm ($N–CH_2$) after introduction of the N-ligands.

The introduction of the organometallic moieties did not induce drastic changes. In fact the metal content is small and therefore since the spectra are dominated by the propyl chain signal it will mask any resonances from other species in lower concentration. A similar effect has already been described previously [37,38].

Fig. 3 shows the ^{29}Si CP MAS NMR spectra for pristine calcined **MCM***, **MCM-Pr-Cl*** (**2***), and the N-ligand derivatized **MCM-Pr-L$_2$** (**4**). Unmodified **MCM** displays two broad convoluted resonances in the ^{29}Si CP MAS NMR spectrum at −110 and −102 ppm, assigned to Q^4 and Q^3 species of the silica framework, respectively, [$Q^n = Si(OSi)_n(OH)_{4-n}$]. The Q^2 species are not observed although their existence cannot be neglected. The Q^3 sites are associated with the single silanols Si–OH (including hydrogen-bonded silanols), while the Q^2 sites correspond to the geminal silanols ($Si–(OH)_2$). The ^{29}Si CP MAS spectra of **MCM-Pr-Cl*** (**2***) and **MCM-Pr-L$_2$** (**4**) also display two broad signals at −58 and −66 ppm, assigned to T^2 and T^3 organosilica species, respectively, [$T^n = RSi(OSi)_n(OEt)_{3-n}$]. The T^1 environment, at −46 ppm, was only detected in the spectrum of **MCM-Pr-Cl*** (**2***). Introduction of the organometallic fragment [$Mo(\eta^3\text{-}C_3H_5)Br(CO)_2$] does not significantly change the ^{29}Si CP MAS-DD NMR spectra, as expected.

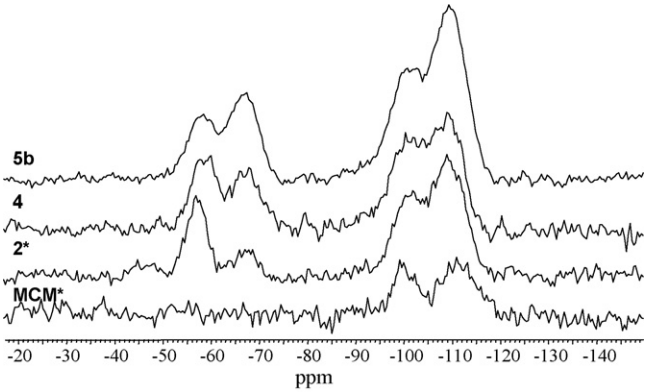

Fig. 3. ^{29}Si CP MAS NMR spectra for calcined **MCM***, **MCM-Pr-Cl*** (**2***), **MCM-Pr-L$_2$** (4) and **MCM-Pr-L$_2$-Mo** (**5b**).

The comparison of the spectra of these materials shows that the in situ grafting of the assorted organic building blocks results in the reduction of the Q^3 resonances, with a concomitant increase of the Q^4 resonance compared to the parent mesoporous sample (**MCM**), confirming that those species were grafted successfully. This trend is kept throughout the complete process and independently of the synthetic pathway adopted.

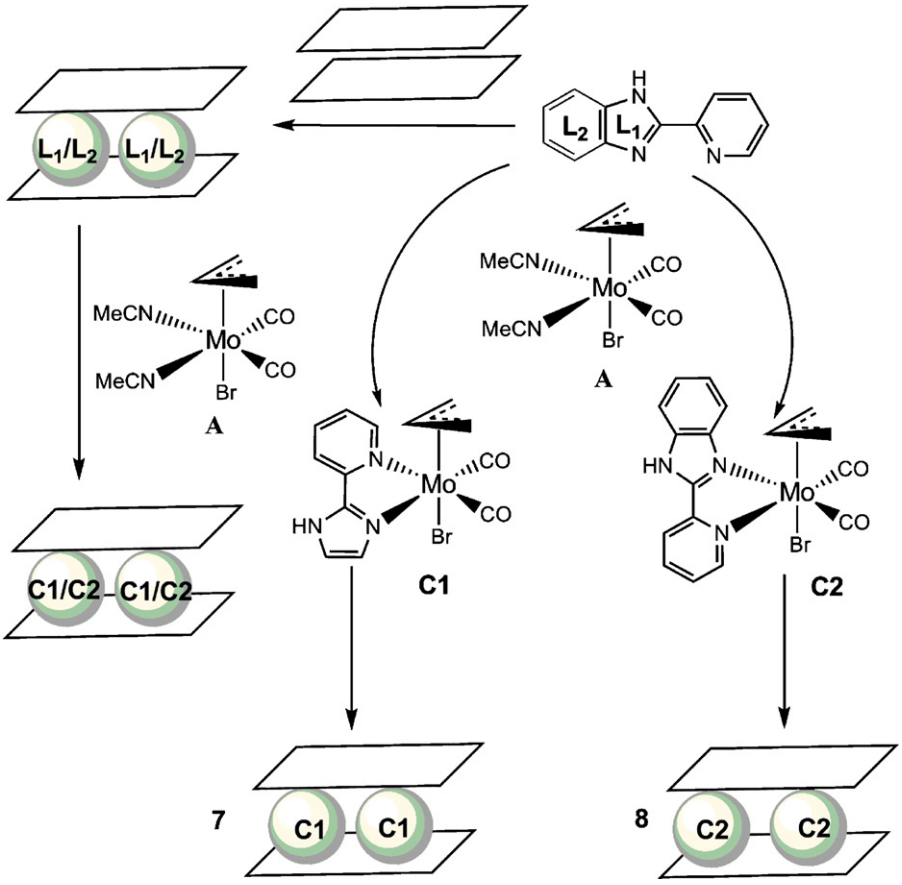

Scheme 3. Schematic procedure for the synthesis of **HTC** materials.

3.2. Hydrotalcite materials

The commercial Mg/Al HTC lamellar material, prior to any manipulation, was calcined at 823 K during 4 h, to eliminate the CO_3^{2-} anions in the interlayer region, as described previously [7]. The structure of the lamellar material collapses, but can be rebuilt [39]. The procedure to be followed is sketched in Scheme 3, showing the two parallel pathways where either the deprotonated ligands (left) or the deprotonated complexes (right) are intercalated between the layers.

Analysis of the XRD powder patterns (not shown) obtained for the starting lamellar materials shows typical patterns of reasonably well ordered materials, exhibiting sharp and symmetric 0 0 3 reflections [12]. The peaks were indexed to a rhombohedral symmetry.

The reconstruction of the layered structure was attempted by deprotonating the ligands (Scheme 3, left) or the complexes (Scheme 3, right) with NaOH. Analysis of the XRD data of the materials obtained in all cases revealed an ordered structure with d parameters of 7.6 Å, which indicate that the intercalated anions are OH^-, instead of the anions of the ligands **L_1**, **L_2** or the complexes **C1**, **C2**.

The FTIR spectra of both lamellar materials **HTC-MoL_1** (**7**) and **HTC-MoL_2** (**8**) showed the two strong ν(C≡O) vibrational modes of the organometallic fragment at around 1935 and 1839 cm^{-1} in **7** and 1932 and 1837 cm^{-1} in **8**, as well as the ν(C=N) modes of the coordinated ligand (1671 cm^{-1} in **7**, 1637 cm^{-1} in **8**). Also, the molybdenum loadings for the organometallic composite materials **7** and **8** were found to be 3.32 and 7.08 wt% (0.35 and 0.74 mmol g^{-1}), respectively, showing that high metal loadings were achieved.

The solid state ^{13}C CP MAS-DD NMR spectra of **7** showed two well defined peaks at 38.6 and 170.3 ppm, assigned to one carbon of the allyl group and to the carbonyl groups (see Scheme 3). The other peaks were not well resolved. In material **8**, two peaks assigned to allylic carbon atoms were observed at 59.9 and 73.7 ppm, and another peak at 170.3 to the carbonyl groups. Other peaks from aromatic carbon atoms are observed in the range 118–160 ppm.

These results suggest that, in the two materials, the OH^- anions are intercalated between the layers of HTC and the anionic complexes obtained after deprotonation are held outside the layers by electrostatic interaction, coating the outside of the clay sheets. A similar situation was detected in all the attempts to intercalate the deprotonated ligands and therefore those materials were not further characterized.

3.3. Catalytic studies

All materials were tested as catalyst precursors for olefin epoxidation using *cis*-cyclooctene (cy8) and styrene (sty) as substrates and *t*-butyl hydroperoxide (TBHP in decane) as oxygen donor, in dichloromethane, at 55 °C (see details in Section 2). Almost no reaction took place in the absence of a catalyst, while the addition of a Mo containing compound led to a catalytic process, yielding the epoxides as the only product within 24 h (Table 2, Fig. 4) when cyclooctene was the substrate. In the oxidation of styrene, some secondary reaction products were detected.

The activity of the two complexes **C1** and **C2** has been reported earlier [26] and is modest, with very low conversions and moderate turnover frequencies, namely 159 and 101 mol mol_{Mo}^{-1} h^{-1} for cyclooctene and higher ones (175 and 150 mol mol_{Mo}^{-1} h^{-1}) for styrene. The heterogeneization process leads in general to higher activities, particularly for styrene epoxidation. The two MCM based materials **MCM-Pr-L_1-Mo** (**5a**), **MCM-Pr-L_2-Mo** (**5b**), obtained through a stepwise procedure lead to conversions close to 100%, with high turnover frequencies, specially for styrene with **5b**.

Table 2
Olefin epoxidation of cyclooctene (cy8) and styrene (sty), using TBHP as oxygen donor, in the presence of materials **MCM-Pr-L_n-Mo** (**5**), **MCM-Pr-MoL_n** (**6**), **HTC-MoL_n** (**7**, **8**), and complexes [Mo(η^3-C_3H_5)Br(CO)$_2$(L)] (L = **L_1**, **C1**; **L_2**, **C2**).

Material/complex[a]	Substrate	Conv.[b] (%)	TOF[c] (mol mol_{Mo}^{-1} h^{-1})
MCM-Pr-L_1-Mo (**5a**)	cy8	95/99[d]	358/449
	sty	92	244
MCM-Pr-L_2-Mo (**5b**)	cy8	99	233
	sty	95	445
MCM-Pr-MoL_1 (**6a**)	cy8	70	77
	sty	89	431
MCM-Pr-MoL_2 (**6b**)	cy8	60	51
	sty	80	401
HTC-MoL_1 (**7**)	cy8	59	311
	sty	82	495
HTC-MoL_2 (**8**)	cy8	60	76
	sty	79	280
C1	cy8	64	159
	sty	54	175
C2	cy8	45	101
	sty	52	150

[a] See Ref. [26].
[b] Cyclooctene conversion after 24 h reaction, at 55 °C.
[c] Turnover frequency calculated at 10 min, at 55 °C.
[d] Cyclooctene conversion after 48 h reaction (second run of the catalyst), at 55 °C.

The materials obtained in the alternative one step synthesis, **MCM-Pr-MoL_1** (**6a**) and **MCM-Pr-MoL_2** (**6b**), display lower conversions (between 60% and 89%) but comparable turnover frequencies for styrene.

The HTC based materials displayed conversions higher for styrene (82%, 79% vs. 54%, 52%), but closer to those of the complexes in homogeneous conditions for cyclooctene (59%, 60% vs. 64%, 45%), although with higher turnover frequencies. Since the catalyst precursors were not intercalated between the layers of the clay, it was thought that lixiviation might take place during catalysis.

Some of the materials were analyzed for their molybdenum content at the end of the catalytic cycle.

For instance, the percentage of molybdenum dropped from 6.21% to 5.71% in **MCM-Pr-L_1-Mo** (**5a**) and from 0.44% to 0.43% in **MCM-Pr-MoL_1** (**6a**), after running the catalysis experiment. For the HTC materials, the analogous drop was from 7.08% to 6.52% in **HTC-MoL_2** (**8**). These values indicate a very small extent of lixiviation of the catalyst from the solid material in both cases.

Also, another load of substrate and TBHP was added to **MCM-Pr-L_1-Mo** (**5a**) and the conversion and TOFs increased slightly, when compared with the results of the first run, suggesting that the material can be reused.

It is thought that the first step of the reaction involves the oxidation of the Mo(II) precursor species to Mo(VI) derivatives, with loss of CO and allyl, but keeping the bidentate ligand [23]. The low activ-

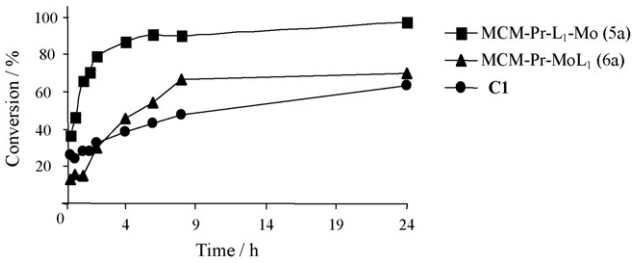

Fig. 4. Conversion of cyclooctene using TBHP as oxygen donor, in the presence of **MCM-Pr-L_1-Mo** (**5a**), **MCM-Pr-MoL_1** (**6a**) and complex [Mo(η^3-C_3H_5)Br(CO)$_2$(L_1)] (**C1**).

ity of the parent complexes in homogeneous phase was ascribed to the presence of the NH groups [26], which might deactivate the catalyst by entering relatively strong hydrogen bond interactions with some molecules, namely the TBHP oxidant. This group has disappeared upon reaction with the chloropropyl arm when immobilizing the complexes in MCM and is probably engaged in strong electrostatic interactions with the cationic HTC layers, allowing a more efficient reactivity toward the oxidant in the first step of the reaction (oxidation to Mo(VI) and formation of the active intermediate).

These ideas are supported by a closer look at the activities of [Mo(η^3-C_3H_5)X(CO)$_2$(N–N)] (X = Cl, Br) precursor complexes with different N–N nitrogen bidentate ligands in homogeneous phase or supported in MCM-41 by a process similar to the one described above (when available; TOFs and conversions of cyclooctene are collected in Table S1) [40,41]. Complexes derived from diimines exhibit in general very high TOFs (~300–400 mol mol$_{Mo}^{-1}$ h^{-1}) and conversions (~100, except the extremely bulky ^{i}Pr derivative); on the other hand, the conversions of the dipyridylamine and 2,2′-bisimidazole complexes are only 64% and 33%, and the TOFs 57 and 29 mol mol$_{Mo}^{-1}$ h^{-1}, respectively. These are the ligands bearing N–H groups, which can be directly compared with **C1** and **C2** (see Table 2), which have similar conversions, though higher TOFs.

For the same diimine, without N–H groups, the immobilization of the complexes in MCM-41 led to a decrease in both the conversion and turnover frequencies. The exception to this behavior has been observed when the bidentate nitrogen ligands are small, leaving plenty of space within the channels, as described for the complexes of the $C_5H_4NCH{=}N\{(CH_2)_3CH_3\}$ ligand with another Mo(II) fragment [42]. In this system, however, the complexes already exhibited a high catalytic activity in homogeneous conditions.

Other Mo(II) complexes derived from Cp′Mo(CO)$_3$X (Cp′ = Cp, Cp*; X = Cl, Me) are also active precursors for cyclooctene epoxidation in the presence of TBHP. Conversions are often 100%, and TOFs depend on conditions, but may be as high as 4000 mol mol$_{Mo}^{-1}$ h^{-1}. As a drawback, these Cp′ based systems are in general less stable in the experimental conditions [43–46].

4. Conclusions

The immobilization of the two complexes [Mo(η^3-C_3H_5)Br(CO)$_2$(L)] (L = **L$_1$**, **C1**, and **L$_2$**, **C2**) inside MCM-41 was successfully achieved by the two different routes, as confirmed by several techniques. The channel structure is kept and the empty space inside the pores remains large enough to allow for catalysis to occur. The stepwise synthetic procedure, starting with the reaction of the ligand with a reactive arm hanging from the walls, followed by reaction with the molybdenum complex [Mo(η^3-C_3H_5)Br(CO)$_2$(NCMe)$_2$], afforded a material much richer in molybdenum than a one step procedure, where the complexes reacted directly with the same pendant arm. The catalytic activity in the olefin epoxidation of these materials was much higher than that of the initial complexes, namely for styrene oxidation.

On the other hand, the planned intercalation of the deprotonated complexes **C1** and **C2** (see Scheme 3) as interlayer anions of HTC did not result, neither in a stepwise reaction (intercalation of the anionic ligands, followed by reaction with [Mo(η^3-C_3H_5)Br(CO)$_2$(NCMe)$_2$]) nor in a one step procedure (intercalation of the deprotonated complexes). Indeed, in the basic medium required to form the anions (easier in the complexes than in the free ligands), the anion that intercalated was OH^-, as deducted from the interlayer space. The adsorption of the complexes seemed to take place in the outside of the HTC layers, so that the resulting material exhibited catalytic activity in the olefin epoxidation reaction.

Acknowledgements

We thank FCT and PIDAC (Project PTDC/QUI/71576/2006) for financial support. MSS (SFRH/BD/48640/2008) thanks FCT for a research grant.

Appendix A. Supplementary data

Supplementary data associated with this article can be found, in the online version, at doi:10.1016/j.molcata.2010.02.008.

References

[1] M.H. Valkenberg, W.F. Hölderich, Catal. Rev. 44 (2002) 321–374.
[2] A. Taguchi, F. Schüth, Micropor. Mesopor. Mater. 77 (2005) 1–45.
[3] C.T. Kresge, M.E. Leonowicz, W.J. Roth, J.C. Vartuli, J.S. Beck, Nature 359 (1992) 710–712.
[4] J.S. Beck, J.C. Vartuli, W.J. Roth, M.E. Leonowicz, C.T. Kresge, K.D. Schmitt, C.T.W. Chu, D.H. Olson, E.W. Sheppard, S.B. McCullen, J.B. Higgins, J.L. Schlenker, J. Am. Chem. Soc. 114 (1992) 10834–10843.
[5] D.M. Ford, E.E. Simanek, D.F. Shantz, Nanotechnology 16 (2005) S458–S475.
[6] C.D. Nunes, M. Pillinger, A.A. Valente, I.S. Gonçalves, J. Rocha, P. Ferreira, F.E. Kühn, Eur. J. Inorg. Chem. (2002) 1100–1107.
[7] M. Pillinger, C.D. Nunes, P.D. Vaz, A.A. Valente, I.S. Gonçalves, P.J.A. Ribeiro-Claro, J. Rocha, L.D. Carlos, F.E. Kühn, Phys. Chem. Chem. Phys. 4 (2002) 3098–3105.
[8] T.A. Fernandes, C.D. Nunes, P.D. Vaz, M.J. Calhorda, P. Brandão, J. Rocha, I.S. Gonçalves, A.A. Valente, L.P. Ferreira, M. Godinho, P. Ferreira, Micropor. Mesopor. Mater. 112 (2008) 14–25.
[9] J. Gimenez, C.D. Nunes, P.D. Vaz, A.A. Valente, P. Ferreira, M.J. Calhorda, J. Mol. Catal. A 256 (2006) 90–98.
[10] C.D. Nunes, A.A. Valente, M. Pillinger, A.C. Fernandes, C.C. Romão, J. Rocha, I.S. Gonçalves, J. Mater. Chem. 12 (2002) 1735–1742.
[11] (a) S.P. Newman, W. Jones, New J. Chem. (1998) 105–115;
(b) S.P. Newman, S.J. Williams, P.V. Coveney, W. Jones, J. Phys. Chem. B 102 (1998) 6710–6719.
[12] A.I. Khan, D. O'Hare, J. Mater. Chem. 12 (2002) 3191–3198.
[13] J.-C. Dupin, H. Martinez, C. Guimon, E. Dumitriu, I. Fechete, Appl. Clay Sci. 27 (2004) 95–106.
[14] M. Vasconcellos-Dias, C.D. Nunes, P.D. Vaz, P. Ferreira, M.J. Calhorda, Eur. J. Inorg. Chem. (2007) 2917–2925.
[15] (a) S. Gago, M. Pillinger, A.A. Valente, T.M. Santos, J. Rocha, I.S. Gonçalves, Inorg. Chem. 43 (2004) 5422–5431;
(b) S. Gago, M. Pillinger, T.M. Santos, J. Rocha, I.S. Gonçalves, Eur. J. Inorg. Chem. (2004) 1389–1395.
[16] G. Negrón, N. Guerrra, L. Lomas, R. Gaviño, J. Cárdenas, Arkivoc xi (2003) 179–184.
[17] (a) R.G. Hayter, J. Organomet. Chem. 13 (1968), Pl–P3;
(b) H. tom Dieck, H. Friedel, J. Organomet. Chem. 14 (1968) 375–385.
[18] H.-U. Blaser, A. Indolese, A. Schnyder, Curr. Sci. 78 (2000) 1336–1344.
[19] (a) Y. Yamaguchi, K. Ogata, K. Kobayashi, T. Ito, Dalton Trans. (2004) 3982–3990;
(b) P.K. Baker, Adv. Organomet. Chem. 40 (1996) 45.
[20] D. Morales, J. Pérez, L. Riera, V. Riera, R. Corzo-Suárez, S. García-Granda, D. Miguel, Organometallics 21 (2002) 1540–1545.
[21] V.S. Joshi, M. Nandi, H. Zhang, B.S. Haggerty, A. Sarkar, Inorg. Chem. 32 (1993) 1301–1303.
[22] (a) B.M. Trost, M. Lautens, J. Am. Chem. Soc. 104 (1982) 5543–5545;
(b) B.M. Trost, M. Lautens, J. Am. Chem. Soc. 109 (1987) 1469–1478;
(c) B.M. Trost, C.A. Merlic, J. Am. Chem. Soc. 112 (1990) 9590–9600.
[23] J.C. Alonso, P. Neves, M.J. Pires da Silva, S. Quintal, P.D. Vaz, C. Silva, A.A. Valente, P. Ferreira, M.J. Calhorda, V. Félix, M.G.B. Drew, Organometallics 26 (2007) 5548–5556.
[24] (a) J.-M. Brégeault, Dalton Trans. (2003) 3289–3302;
(b) K.A. Jørgensen, Chem. Rev. 89 (1989) 431–458.
[25] (a) M.K. Trost, R.G. Bergman, Organometallics 10 (1991) 1172–1178;
(b) A.M. Martins, C.C. Romão, M. Abrantes, M.C. Azevedo, J. Cui, A.R. Dias, M.T. Duarte, M.A. Lemos, T. Lourenço, R. Poli, Organometallics 24 (2005) 2582–2589;
(c) A.A. Valente, J.D. Seixas, I.S. Gonçalves, M. Abrantes, M. Pillinger, C.C. Romão, Catal. Lett. 101 (2005) 127–130.
[26] M.S. Saraiva, S. Quintal, F.C.M. Portugal, T.A. Lopes, V. Félix, J.M.F. Nogueira, M. Meireles, M.G.B. Drew, M.J. Calhorda, J. Organomet. Chem. 693 (2008) 3411–3418.
[27] B. Chiswell, F. Lions, B.S. Morris, Inorg. Chem. 3 (1964) 110–114.
[28] M. Kruk, M. Jaroniec, Langmuir 13 (1997) 6267–6273.
[29] M. Kruk, V. Antochshuk, M. Jaroniec, J. Phys. Chem. B 103 (1999) 10670–10683.
[30] P. Beaudot, M.E. De Roy, J.P. Basse, Chem. Mater. 16 (2004) 935–945.

[31] B. Marler, U. Oberhagemann, S. Voltmann, H. Gies, Micropor. Mesopor. Mater. 6 (1996) 375–383.
[32] W. Hammond, E. Prouzet, S.D. Mahanti, T.J. Pinnavaia, Micropor. Mesopor. Mater. 27 (1999) 19–25.
[33] S.J. Gregg, K.S.W. Sing, Adsorption, Surface Area and Porosity, 2nd ed., Academic Press, London, 1982.
[34] M.D. Alba, A. Becerro, J. Klinowski, J. Chem. Soc. Faraday Trans. 92 (1996) 849–854.
[35] A.A. Romero, M.D. Alba, W. Zhou, J. Klinowski, J. Phys. Chem. B 101 (1997) 5294–5300.
[36] M. Kruk, M. Jaroniec, Langmuir 15 (1999) 5410–5413.
[37] P. Ferreira, C.D. Nunes, P.D. Vaz, N. Bion, P. Brandão, J. Rocha, Prog. Solid State Chem. 33 (2005) 163–170.
[38] C.D. Nunes, P.D. Vaz, P. Brandão, J. Rocha, P. Ferreira, N. Bion, M.J. Calhorda, Micropor. Mesopor. Mater. 95 (2006) 104–111.
[39] S. Gago, M. Pillinger, R.A. Sá Ferreira, L.D. Carlos, T.M. Santos, I.S. Gonçalves, Chem. Mater. 17 (2005) 5803–5809.
[40] J.C. Alonso, P. Neves, C. Silva, A.A. Valente, P. Brandão, S. Quintal, M.J.V. de Brito, P. Pinto, V. Felix, M.G.B. Drew, J. Pires, A.P. Carvalho, M.J. Calhorda, P. Ferreira, Eur. J. Inorg. Chem. (2008) 1147–1156.
[41] M.S. Saraiva, N.L. Dias Filho, C.D. Nunes, P.D. Vaz, T.G. Nunes, M.J. Calhorda, Micropor. Mesopor. Mater. 117 (2009) 670–677.
[42] M. Vasconcellos-Dias, C.D. Nunes, P.D. Vaz, P. Ferreira, P. Brandão, V. Félix, M.J. Calhorda, J. Catal. 256 (2008) 301–311.
[43] M. Abrantes, A.M. Santos, J. Mink, F.E. Kühn, C.C. Romão, Organometallics 22 (2003) 2112–2118.
[44] F.E. Kühn, M. Abrantes, A.M. Santos, Chem. Rev. 106 (2006) 2445–2475.
[45] J. Zhao, K.R. Jain, E. Herdtweck, F.E. Kühn, Dalton Trans. (2007) 5567–5571.
[46] K.R. Jain, F.E. Kühn, Dalton Trans. (2008) 2221–2227.